

Hot and Cooled baryons in SPH simulations of galaxy clusters: physics and numerics

S. Borgani^{1,2}, K. Dolag³, G. Murante^{4,1}, L.-M. Cheng⁵, V. Springel³,
A. Diaferio⁶, L. Moscardini⁷, G. Tormen⁸, L. Tornatore^{9,2} & P. Tozzi^{10,2}

¹ Dipartimento di Astronomia dell'Università di Trieste, via Tiepolo 11, I-34131 Trieste, Italy (borgani@ts.astro.it)

² INFN – National Institute for Nuclear Physics, Trieste, Italy

³ Max-Planck-Institut für Astrophysik, Karl-Schwarzschild Strasse 1, Garching bei München, Germany (kdolag,volker@mpa-garching.mpg.de)

⁴ INAF, Osservatorio Astronomico di Torino, Strada Osservatorio 20, I-10025 Pino Torinese, Italy (giuseppe@to.astro.it)

⁵ Institute of Theoretical Physics, Chinese Academy of Sciences, Zhong Guan Cun South 4th Street, 1A P.O.Box 2735, Beijing 100080, China (clm@itp.ac.cn)

⁶ Dipartimento di Fisica Generale “Amedeo Avogadro”, Università degli Studi di Torino, Torino, Italy (diaferio@ph.unito.it)

⁷ Dipartimento di Astronomia, Università di Bologna, via Ranzani 1, I-40127 Bologna, Italy (lauro.moscardini@unibo.it)

⁸ Dipartimento di Astronomia, Università di Padova, vicolo dell'Osservatorio 2, I-35122 Padova, Italy (tormen@pd.astro.it)

⁹ SISSA/International School for Advanced Studies, via Beirut 4, 34100 Trieste, Italy (torna@sissa.it)

¹⁰ INAF, Osservatorio Astronomico di Trieste, via Tiepolo 11, I-34131 Trieste, Italy (tozzi@ts.astro.it)

Accepted ????. Received ????. in original form ???

ABSTRACT

We discuss an extended set of Tree+SPH simulations of the formation of clusters of galaxies, with the goal of investigating the interplay between numerical resolution effects and star-formation/feedback processes. Our simulations were all carried out in a concordance Λ CDM cosmology and include radiative cooling, star formation, and energy feedback from galactic winds. The simulated clusters span the mass range $M_{\text{vir}} \simeq (0.1 - 2.3) \times 10^{15} h^{-1} M_{\odot}$, with mass resolution varying by several decades. At the highest achieved resolution, the mass of gas particles is $m_{\text{gas}} \simeq 1.5 \times 10^7 h^{-1} M_{\odot}$, which allows us to resolve the virial region of a Virgo-like cluster with more than 2 million gas particles and with at least as many dark-matter (DM) particles. Our resolution study confirms that, in the absence of an efficient feedback mechanism, runaway cooling leads to about 35 per cent of baryons in clusters to be locked up in long lived stars at our highest resolution, with no evidence of convergence. However, including feedback causes the fraction of cooled baryons to converge at about 15 per cent already at modest resolution, which is much closer to the typical values inferred from observational data. Feedback also stabilizes other gas-related quantities, such as radial profiles of entropy, gas density and temperature, against variations due to changes in resolution. Besides effects of mass resolution, we also investigate the influence of the gravitational force softening length, and that of numerical heating of the gas induced by two-body encounters between DM and lighter gas particles. We also show that simulations where more DM than gas particles are used, such that $m_{\text{gas}} \simeq m_{\text{DM}}$, show a significantly enhanced efficiency of star formation at $z \gtrsim 3$, but they accurately reproduce at $z = 0$ the fraction of cooled gas and the thermodynamical properties of the intra-cluster gas. Our results are important for establishing and delineating the regime of numerical reliability of the present generation of hydrodynamical simulations of galaxy clusters.

Key words: Cosmology: numerical simulations – galaxies: clusters – hydrodynamics

1 INTRODUCTION

Within the hierarchy of cosmic structures, clusters of galaxies mark an interesting transition between the large-scale regime, where the dynamics is dominated by gravity, and the small-scale regime, where complex astrophysical processes, such as gas cooling, star formation and energetic feedback processes, control the formation

and evolution of galaxies (e.g. Rosati et al. 2002; Voit 2005, for recent reviews). If gravity were the only player at the scales relevant for galaxy clusters, then the overall thermal content of baryons would be completely determined by the processes of adiabatic compression and shock heating within the dark-matter (DM) dominated potential wells (e.g. Kaiser 1986; Tozzi & Norman 2001). Since gravity has no characteristic scales, this scenario predicts

that galaxy clusters and groups of different mass should appear as scaled versions of each other, with only weak residual trends due to a variation of the halo concentration with mass. However, a number of observational facts highlight that the evolution of cosmic baryons within clusters must be influenced by physical processes other than gravity. First, scaling relations between X-ray observables demonstrate that groups and poor clusters have a lower content of diffuse hot gas than rich clusters, and that they lie on a comparatively higher adiabat (e.g. Markevitch 1998; Arnaud & Evrard 1999; Ettori et al. 2002; Ponman et al. 2003; Osmond & Ponman 2004). Second, the bulk of the gas in central cluster regions lies at a temperature which is never observed to fall below $1/3$ – $1/2$ of the virial temperature, despite the fact that the cooling time of this gas is much shorter than the Hubble time (e.g. Peterson et al. 2001; Molendi & Pizzolato 2001; Böhringer et al. 2002). Third, the fraction of baryons in the stellar phase within clusters is consistently rather small, around ~ 10 per cent (e.g. Balogh et al. 2001), with a tendency for poor clusters and groups to have a somewhat higher amount of stars (e.g. Lin et al. 2003; Rines et al. 2004).

These observational evidences indicate the existence of a delicate interplay between the physical processes which determine the evolution of the inter-galactic (IGM) and intra-cluster (ICM) media. Including hydrodynamical effects beyond ordinary gas dynamics, such as gas cooling, star formation and associated feedback processes, in simulation models is however met with substantial difficulty. While analytical and semi-analytical calculations can provide very useful guidelines for the expected effects (e.g. Tozzi & Norman 2001; Bower et al. 2001; Babul et al. 2002; Voit et al. 2003; Lapi et al. 2005), we nevertheless rely on such simulation models, because the non-linearity of the physics and the geometrical complexity of cluster dynamics can usually only be captured in full by direct simulation. This makes it extremely important to obtain an in-depth understanding of the robustness of the numerical methods employed, of the assumptions behind them, and of the sensitivity of numerical predictions for observable quantities on the adopted numerical parameters and approximations.

One important validation test is to compare different simulation codes and different schemes for solving hydrodynamics with each other. For a single code, additional control tests that scrutinize the robustness of the predictions against resolution and different implementations of sub-resolution processes are highly desirable as well. An example for the importance of such tests is represented by radiative cooling, which is well known to exhibit a runaway character: cooling leads to an increase of the gas density, which, in turn, increases the cooling efficiency. Consistently, hydrodynamical cosmological simulations have shown that the fraction of gas that cools down and becomes available for star formation is much larger than indicated by observations (e.g. Katz & White 1993; Sugimotohara & Ostriker 1998; Pearce et al. 2000; Lewis et al. 2000; Yoshida et al. 2002), a tendency that increases with resolution (e.g. Balogh et al. 2001; Tornatore et al. 2003). Solving this problem apparently requires the introduction of suitable feedback physics which reduces the fraction of cooled gas and stabilizes its value against numerical resolution.

So far, detailed comparisons between different cosmological hydrodynamical codes have been restricted to the case of non-radiative simulations (e.g. Kang et al. 1994; Frenk et al. 1999; O’Shea et al. 2005). While these comparisons have shown a reasonable level of agreement, some sizeable differences have been found in the profiles of thermodynamic quantities (e.g., entropy) when simulations of galaxy clusters performed with Eulerian and Lagrangian codes were compared (Frenk et al. 1999). A limited

number of studies have been presented so far which were aimed at discussing the effect of resolution and different implementations of cooling/star-formation physics within a single code. For instance, Kay et al. (2002) compared different implementations of star formation. They concluded that different prescriptions provide broadly consistent results, although the amount of cooled gas is always much higher than observed. They also verified that this over-cooling can be partly ameliorated by resorting to either kinetic or thermal feedback.

Besides checking the influence of different parameterizations of physical effects, it is crucial to have purely numerical effects well under control, such as those originating from mass resolution and force softening. Detailed studies have been presented about the determination of an optimum softening for purely collisionless simulations (e.g. Power et al. 2003; Zhan 2005), usually based on a compromise between the desire of obtaining an accurate estimate of the accelerations together with high spatial resolution, and at the same time, the need to suppress two-body relaxation and the formation of bound particle pairs if too small a softening is chosen (e.g. Thomas & Couchman 1992).

The situation is more complicated for hydrodynamical simulations, where energy can be spuriously transferred from the collisionless to the collisional component, thereby affecting the evolution of the gas. As Steinmetz & White (1997) have shown, this can happen when the gas particles are substantially lighter than the dark matter particles, such that the former receive a systematic energy transfer in two-body encounters, leading to artificial heating of the gas. As a result, a lower-limit exists for the required mass resolution in order to provide a correct description of gas cooling within halos of a given mass.

In a series of papers (e.g., Borgani et al. 2004; Dolag et al. 2004; Murante et al. 2004; Ettori et al. 2004; Diaferio et al. 2005; Cheng et al. 2005; Ettori et al. 2005) we have presented results on the properties of galaxy clusters, extracted from a large-scale simulation and performed with the GADGET-2 code (Springel et al. 2001; Springel 2005), including the star formation and feedback model of Springel & Hernquist (2003a,b). This model is formulated as a sub-resolution model to account for the multiphase nature of the interstellar medium (ISM), and contains a phenomenological model of energy feedback from galactic winds triggered by supernova (SN) explosions (see Section 2). The present paper is specifically aimed at discussing the numerical robustness of the results we obtained, by analysing an extended set of re-simulations of galaxy clusters, spanning a fairly large range both in cluster mass and numerical resolution. More specifically, we will primarily address the following two questions: (a) How does numerical resolution affect the properties of the diffuse baryons and the distribution of star formation within clusters? (b) How large is the impact of artificial heating and how can numerical parameters (i.e., force softening and mass-ratio between gas and DM particles) be chosen to minimize its effect?

The plan of the paper is as follows. In Section 2, we provide the details of the simulated clusters. We analyze in Section 3 the effects of changing resolution over a fairly large range, up to a factor 45 in particle masses. In this section we will also discuss how the adopted feedback from galactic winds affects the resolution dependence of measured properties for the simulated clusters. In Section 4, we discuss the role of different sources of numerical heating. Finally, we will summarize our results and draw our main conclusions in Section 5.

Cluster run	M_{vir}	R_{vir}	T_{mw}
Set #1			
CL1	13.7	2.3	5.7
CL2	2.9	1.4	2.3
CL3	2.4	1.3	2.1
CL4	1.6	1.1	1.7
Set #2			
CL5	14.9	2.4	7.0
CL6	1.1	1.0	1.4

Table 1. Basic properties of the 6 clusters belonging to the two sets of simulations. Column 1: cluster name; Column 2: virial mass, defined as the total mass contained within the virial radius (units of $10^{14}h^{-1}M_{\odot}$); Column 3: virial radius, defined as the radius encompassing an average density equal to the virial density predicted for the assumed cosmology (see also text; units of $h^{-1}\text{Mpc}$); Column 4: mass-weighted temperature computed within R_{vir} (units of keV). All the values reported refer to the reference runs of both simulation sets (see text).

2 THE SIMULATIONS

Our simulations were carried out with GADGET-2 (Springel 2005), an improved version of the parallel Tree-SPH simulation code GADGET (Springel et al. 2001). It uses an entropy-conserving formulation of SPH (Springel & Hernquist 2002), and includes radiative cooling, heating by a uniform redshift-evolving UV background (Haardt & Madau 1996), and a treatment of star formation and feedback processes. The prescription of star formation is based on a sub-resolution model to account for the multi-phase nature of the interstellar medium (ISM), where the cold phase of the ISM is the reservoir of star forming gas (Springel & Hernquist 2003a, SH03 hereafter). As for the feedback, SH03 followed a phenomenological scheme to include the effect of galactic winds, whose velocity, v_w , scales with the fraction η of the SN-II feedback energy that contributes to the winds, as $v_w \propto \eta^{1/2}$ (see eq.[28] in SH03). The total energy provided by SN-II is computed by assuming that they originate from stars with mass $> 8M_{\odot}$ for a Salpeter (1955) initial mass function (IMF), with each SN releasing 10^{51} ergs. As discussed in the following, we will assume $\eta = 0.5$ and 1, yielding $v_w \simeq 340$ and 480 km s^{-1} , respectively, while we will also explore the effect of switching off galactic winds altogether.

We consider two sets of clusters, which have been selected from different parent cosmological boxes. Initial conditions for both sets have been generated using the Zoomed Initial Condition (ZIC) technique by Tormen et al. (1997). This technique increases the mass resolution in a suitably chosen high-resolution Lagrangian region surrounding the structure to be re-simulated. It then adds additional initial displacements, assigned according to the Zeldovich approximation (e.g. Shandarin & Zeldovich 1989), from the newly sampled high-frequency modes which were not assigned in the low-resolution parent simulation. Furthermore, the mass resolution is progressively degraded in more distant regions, so as to save computational resources while still correctly describing the large-scale tidal field of the cosmological environment.

Once initial positions and velocities are assigned, a DM-only run is performed to check for any contamination of the surroundings of the cluster virial region by heavy particles that may have moved in from the low- to the high-resolution region. If required, the shape of the Lagrangian high-resolution region is optimized by trial and error until any such contamination around the halo of interest is prevented. With a typical number of 3-5 trials, we end up with

Run name	m_{DM}	m_{gas}	ϵ_{PI}	z_{ϵ}
Set #1 LR	46.4	6.93	7.5	2
Set #1 MR	15.5	2.31	5.2	2
Set #1 HR	4.6	0.69	3.5	2
Set #1 VR	1.0	0.15	2.1	2
Set #2	11.3	1.69	5.0	5

Table 2. Parameters defining the two sets of runs (see also text). Column 1: name of the run; Column 2: mass of the high-resolution DM particles (in units of $10^8 h^{-1}M_{\odot}$); Column 3: mass of the gas particles (in units of $10^8 h^{-1}M_{\odot}$); Column 4: Plummer-equivalent gravitational force softening at $z = 0$ in the high-resolution region (units of $h^{-1}\text{kpc}$). Column 5: redshift of transition from physical to comoving softening.

initial conditions which produce a cluster that, at $z = 0$, is free of contaminants out to $(4-6)R_{\text{vir}}$. Once initial conditions are created, we split particles in the high-resolution region into a DM and a gas component, whose mass ratio is set to reproduce the assumed cosmic baryon fraction. Instead of placing them on top of each other, we displace gas and DM particles such that the centre of mass of each parent particle is preserved and the final gas and dark matter particle distributions are interleaved by one mean particle spacing.

2.1 The Set #1

This set includes four clusters, resimulated at different resolutions, with virial mass in the range $M_{\text{vir}} = (1.6-13) \times 10^{14} h^{-1}M_{\odot}$ (CL1 to CL4 in Table 1). These clusters have been extracted from the cosmological hydrodynamical simulation presented by Borgani et al. (2004). The simulation followed 480^3 DM particles and an initially equal number of gas particles, within a box of $192 h^{-1}\text{Mpc}$ on a side, for a flat ΛCDM model with $\Omega_m = 0.3$, $h = 0.7$, $\sigma_8 = 0.8$ and $\Omega_b = 0.04$. With these choices, the masses of the DM and gas particles are $m_{\text{DM}} \simeq 4.6 \times 10^9 h^{-1}M_{\odot}$ and $m_{\text{gas}} \simeq 6.9 \times 10^8 h^{-1}M_{\odot}$, respectively. The force accuracy is set by $\epsilon_{\text{PI}} = 7.5 h^{-1}\text{kpc}$ for the Plummer-equivalent softening parameter, fixed in physical units from $z = 0$ to $z = 2$, and kept fixed in comoving units at higher redshifts.

Since initial conditions of the parent simulations have been generated on a grid, a grid is also used to assign initial displacements for these resimulations. Initial conditions for each cluster are generated at four different mass resolutions, corresponding to the basic resolution of the parent box (low resolution, LR), and to 3 times (medium resolution, MR), 10 times (high resolution, HR) and 45 times (very high resolution, VR) smaller particle masses. The VR run is not carried out for the CL1 cluster, whose large mass would result in a too large computational cost. The gravitational softening in the high-resolution regions is rescaled with the mass of the particles according to $\epsilon_{\text{PI}} \propto m^{1/3}$, where the LR runs were set to have the same softening as used in the parent simulation. In Table 2, we list the masses of the DM and gas particles, as well as the force softening for the different resolutions. At the highest achieved resolution, each cluster is resolved with at least 1.5 million DM particles within the virial radius, with CL2 reaching 2.2 million particles. The reference runs for the clusters of Set #1 have been performed by assuming that 100 per cent of the energy provided by SNe is carried by winds. This gives a wind speed of $v_w \simeq 480 \text{ km s}^{-1}$.

Run name	Description	Applied to:
NW	No winds: winds switched off	CL2-LR,HR; CL4-LR,MR,HR,VR
SW	Strong winds: wind velocity for the Set #2 at the reference value of the Set #1	CL5, CL6
1o8	Eight times heavier gas particles	CL4-VR
S08	SW runs for clusters of the Set #2 with $\sigma_8 = 0.8$	CL5, CL6

Table 3. Description of the name extensions used for the identification of the runs.

2.2 The Set #2

This set includes 2 clusters having mass $\simeq 10^{15} h^{-1} M_\odot$ and $\simeq 10^{14} h^{-1} M_\odot$ (CL5 and CL6 in Table 1, respectively). They have been selected from a larger sample of 20 clusters with masses in the range $5 \times 10^{13} - 2.3 \times 10^{15} h^{-1} M_\odot$, which have been identified in simulations of 9 Lagrangian regions (Dolag et al., in preparation). These systems were extracted from a DM-only simulation with a box size of $479 h^{-1} \text{Mpc}$ of a flat ΛCDM model with $\Omega_m = 0.3$, $h = 0.7$, $\sigma_8 = 0.9$ and $\Omega_b = 0.04$ (Yoshida et al. 2001). Differently from Set #1, the initial displacements were generated using a ‘glass’ (White 1996) for the Lagrangian particle distribution. Only one mass resolution was simulated in this case, corresponding to $m_{\text{DM}} = 1.13 \times 10^9 h^{-1} M_\odot$ and $m_{\text{gas}} = 1.7 \times 10^8 h^{-1} M_\odot$ for dark matter and gas within the high-resolution region, respectively. As such, this mass resolution is about 4 times better than the LR runs, and therefore lies intermediate between the MR and the HR runs of Set #1. The softening length is set to $\epsilon_{\text{P1}} = 5.0 h^{-1} \text{kpc}$, fixed in physical units below $z = 5$, while it is kept fixed in comoving units at higher redshift. The reference runs for clusters of Set #2 assume that 50 per cent of the energy provided by SN (i.e. half of that used for the Set #1) is carried by winds. This gives a wind speed of $v_w \simeq 340 \text{ km s}^{-1}$. Unless otherwise stated, our analysis presented in this paper is restricted to the CL5 and CL6 simulations out of the 20 clusters of the full Set #2. We note that for all of our simulations, we set the smallest allowed value for the SPH smoothing length to $\epsilon_{\text{P1}}/4$.

In summary, our two sets of simulated clusters differ in the following aspects:

- The value of σ_8 changes from 0.8 to 0.9 when going from Set #1 to Set #2. To explicitly check for the effect of changing the normalization σ_8 , we will also analyse additional simulations of the CL5 and CL6 clusters of Set #2 using $\sigma_8 = 0.8$.
- The initial Lagrangian positions of DM and gas particles were taken to be a grid for Set #1 and a glass for Set #2. We will also present results for CL5 of Set #2 using grid initial conditions, to check explicitly for effects due to a grid vs. a glass setup.
- The velocity of the galactic winds is $v_w \simeq 480 \text{ km s}^{-1}$ and 340 km s^{-1} for Set #1 and Set #2, respectively. To address this important difference, we have rerun the CL5 and CL6 clusters from Set #2 with $\sigma_8 = 0.8$ and with the stronger feedback, to make them fully comparable with the clusters of Set #1.
- The transition from physical to comoving softening takes place at $z = 5$ for Set #2 and at $z = 2$ for Set #1. To test the effect of a change of this transition redshift we have rerun CL6 of Set #2 with strong winds, also using the same choice of softening as for Set #1.

We will use the convention that a certain simulation of each cluster is labeled by the name of the cluster itself, followed, when required, by a label which specifies the resolution used. In this way, CL1-MR will indicate the reference run of medium-resolution of

the CL1 cluster from Set #1, while CL5 will designate the reference run of this cluster from Set #2. For the latter, we do not specify the resolution, since clusters from Set #2 are simulated at only one resolution. In addition, a further extension of the name of each run will be provided whenever the run differs from the reference run of the set it belongs to. The list of such extensions and their description is given in Table 3. For instance, CL4-HR indicates the high-resolution run of the CL4 cluster, using the standard setup of Set #1, while CL4-HR-NW stands for the same simulation, but neglecting the effect of galactic winds.

We show in Figure 1 the gas density maps of the six simulated clusters within boxes each having a size of $4R_{\text{vir}}$. The four clusters from the Set #1 are shown in their highest resolution version.

2.3 Basics of the simulation analysis

In the first step of our simulation analysis we determine suitable cluster centers. These are defined as the position of the most bound particle among those grouped together by a FOF algorithm with linking length $b = 0.15$ (in units of the mean interparticle separation in the high-resolution region). Once the center is identified, we apply a spherical overdensity algorithm to determine the virial radius, R_{vir} . We here defined this as the radius that encompasses an average density equal to the virial density for the adopted cosmological model, $\rho_{\text{vir}}(z) = \Delta_c(z)\rho_c(z)$ ($\rho_c(z) = [H(z)/H_0]^2 \rho_{c,0}$ is the critical density at redshift z), where the overdensity $\Delta_c(z)$ is computed as described by Eke et al. (1996), with $\Delta_c(0) \simeq 100$ for the assumed cosmology. The virial mass, M_{vir} , is simply the mass contained within the virial radius. In Table 1, we provide the typical values of R_{vir} , M_{vir} and mass-weighted temperature, T_{mw} , for the six simulated clusters. Profiles of gas-related quantities are computed within 200 equispaced linear radial bins, out to $2R_{\text{vir}}$, starting from a minimum radius which contains 100 gas particles. As shown by Borgani et al. (2002), numerically stable results can be expected for this choice in non-radiative simulations of galaxy clusters.

We identify galaxies in our simulations by applying the SKID algorithm¹ (Stadel 2001) to the distribution of star particles. In the following, we provide a short description of our algorithm, while a more detailed discussion and presentation of tests is provided elsewhere (Murante et al. 2005, in preparation). Briefly, the SKID algorithm works as follows:

- An overall density field is computed by using the distribution of all the particle species, i.e. DM, gas and star particles. The density is estimated with a SPH spline-kernel, using a given number N_{sm} of neighbour particles.
- The star particles are moved along the gradient of the density field in steps of $\tau/2$. When a particle begins to oscillate inside a sphere of radius $\tau/2$, it is stopped. In this way, τ can be interpreted

¹ See <http://www-hpcc.astro.washington.edu/tools/skid.html>

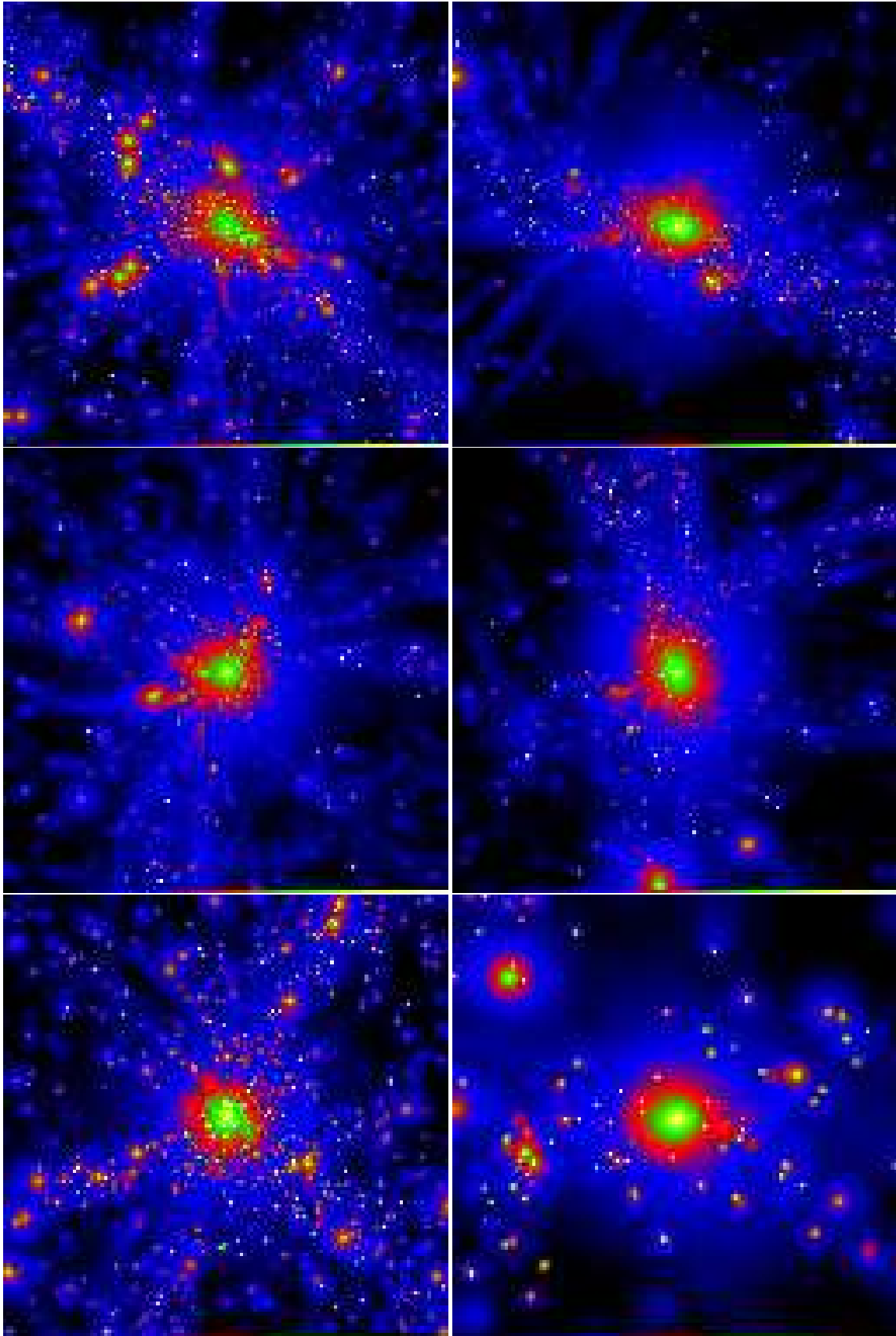


Figure 1. Maps of the gas density for the six simulated clusters, in a region encompassing two virial radii around each cluster centre. Top–left to bottom–right panels are for the CL1 to CL6 clusters. For the clusters belonging to Set #1 (CL1 to CL4), we show maps for the highest resolution runs (HR for CL1 and VR for CL2 to CL4). In all cases, the maps refer to the runs with strong winds (i.e. $v_w \simeq 480 \text{ km s}^{-1}$). The small bright knots mark the “galaxies”, i.e. the places where high density gas is undergoing cooling and star formation.

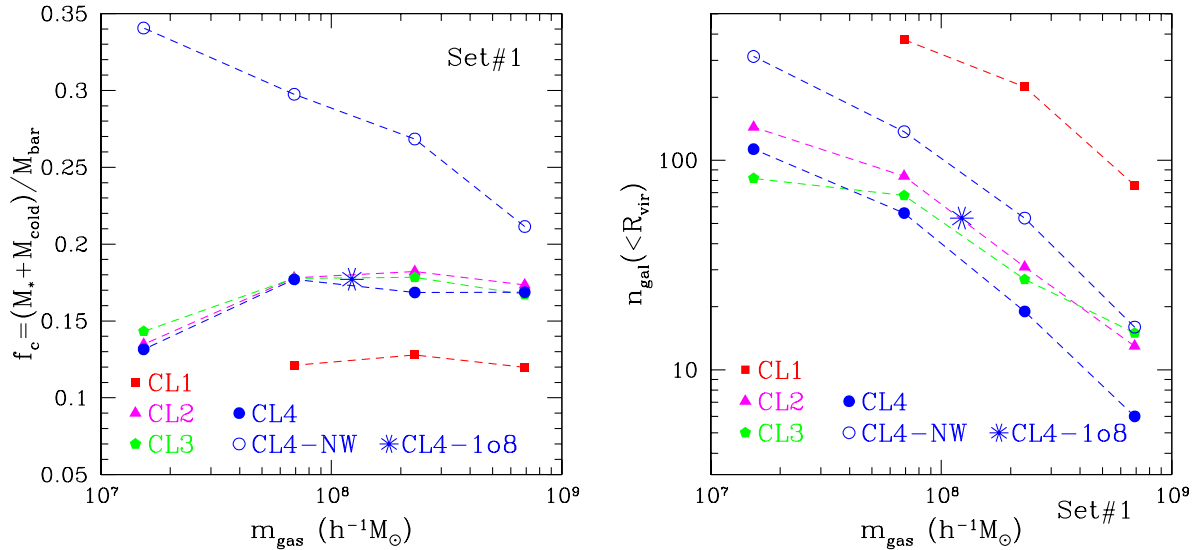


Figure 2. The fraction of cooled baryons f_c (left panel), and the number of galaxies within R_{vir} , as functions of the mass of the gas particle, for the clusters of Set #1 at different resolution. Filled symbols are for the “reference” runs. The open circles are for the runs of the CL4 cluster with wind feedback turned off. The asterisk is for the CL4 run at very high resolution using 8 times heavier gas particles (CL4-1o8), so that the gas particle mass is similar to that of the DM particles in the high-resolution region.

as the typical size of the smallest resolved structure in the distribution of the star particles.

- When all particles have been moved, they are grouped using a friends-of-friends (FOF) algorithm applied to the moved particle positions. The linking length is again $\tau/2$.

- The binding energy of each group identified in this way is computed by accounting for all the particles inside a sphere centered on the center of mass of the group and having radius 2τ (for the moved particles, their initial positions are used in the computation of the potential). This binding energy is then used to remove from the group all the star particles which are recognized as unbound. Finally, we retain such a SKID-group of stars as a galaxy if it contains at least 32 particles after the removal of unbound stars.

The resulting list of objects identified by SKID depends on the choice of two parameters, namely τ and N_{sm} . After many experiments, and resorting to visual inspection in all cases, we found that a complete detection of bound stellar objects requires use of a set of different values of N_{sm} . We used $N_{sm} = 16, 32, 64$, and define a “galaxy” to be the set of star particles which belong to a SKID group with any one of the above N_{sm} values. If a star particle belongs to a SKID group for one value of N_{sm} and to another group for a different N_{sm} , then the groups are “joined” and are considered as forming a single galaxy. All star particles not linked to any galaxy are considered to be part of a diffuse stellar component in the cluster (Murante et al. 2004). As for τ , since it roughly corresponds to the size of the smallest resolved structure, we adopt $\tau = 2.8\epsilon_{\text{PI}}$, which is the scale where the softened force becomes equal to the Newtonian force.

3 THE EFFECT OF MASS RESOLUTION

Checking the stability of simulation results against numerical resolution is always of paramount importance to assess their robustness. For hydrodynamical simulations of clusters that only account

for non-radiative physics, it has been shown that numerically reliable estimates of global cluster properties, such as temperature and X-ray luminosity, are obtained when each halo is resolved with a few tens of thousands of gas particles within the virial region, a resolution which is also enough to result in converged radial profiles for the gas density, temperature and entropy down to a few percent of the virial radius (e.g., Navarro et al. 1995; Borgani et al. 2002, and references therein). However, the situation is considerably less clear when additional physical processes are introduced. For example, the efficiency of radiative cooling in simulations is known to sensitively depend on the adopted mass resolution. At the same time, the effects of feedback from galactic winds may also depend on numerical resolution, and it is unclear whether this resolution dependence favourably counteracts the increasing efficiency of cooling. We generated the initial conditions for Set #1 at four different resolutions precisely for the purpose of checking in detail the resolution-dependence of the non-trivial physical processes included in our simulations.

3.1 Star formation

In Figure 2, we show the dependence of the fraction of cooled baryons and of the number of identified galaxies within R_{vir} on the mass of the gas particles. In the absence of feedback by galactic winds, the CL4 runs develop the typical runaway of cooling as a function of the mass resolution. The fraction of cooled baryons steadily increase from 21 per cent at the lowest resolution to 34 per cent at the highest achieved resolution, with no indication of convergence. A part of the origin of this runaway is illustrated in the left panel of Figure 3, where we show the star formation history for the CL4 runs at the different resolutions, in the absence of winds. Increasing the resolution leads to an earlier onset of star formation within ever smaller first-collapsing halos, and at low redshift, cooling and star formation appear to never enter in any self-regulated

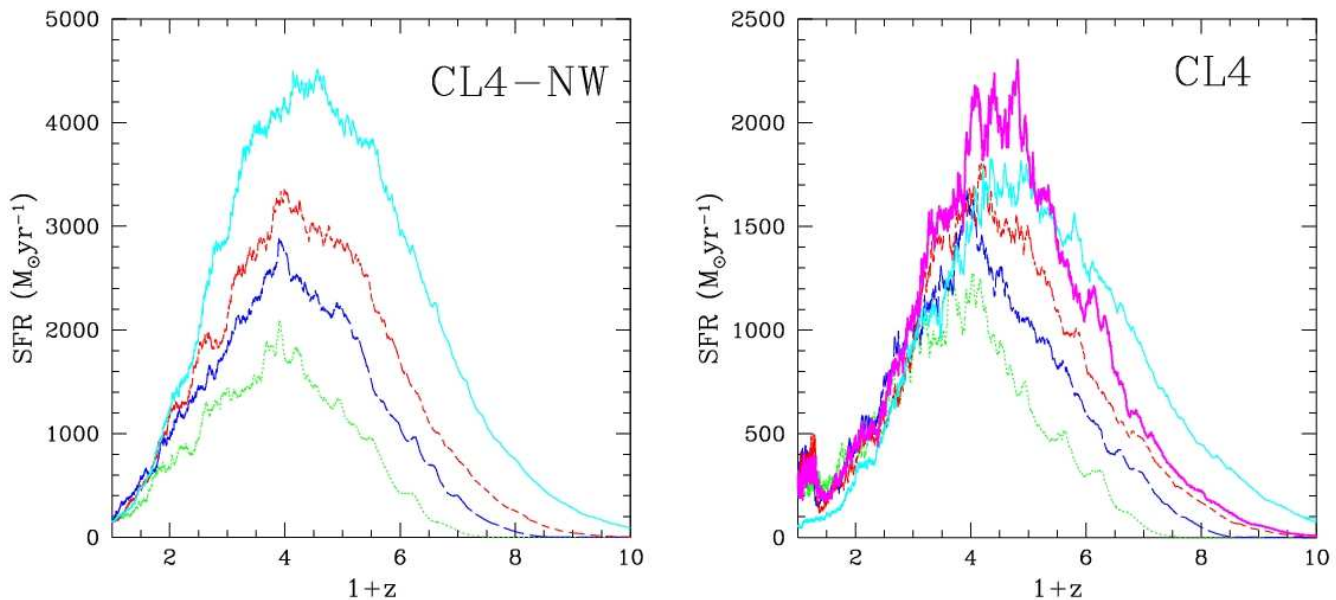


Figure 3. The star formation rate as a function of the mass resolution for the CL4 cluster, both excluding (left panel) and including (right panel) the effect of galactic winds. In both panels, solid, short-dashed, long-dashed, and dotted curves correspond to the VR, HR, MR and LR runs, respectively. In the right panel, the heavy solid curve is for the VR run, where gas particles have nearly the same mass as the DM particles (1o8 run in Table 3). Note the different scales on the vertical axes in the two panels.

regime. As a result, the star formation efficiency progressively increases with resolution at all epochs.

On the other hand, including feedback by galactic winds is quite effective in regulating the process of star formation. In this case, there is no evidence for a systematic increase of the fraction of cooled baryons with increasing resolution. In fact, the three poor clusters have rather similar values of $f_c \sim 15$ per cent, and the massive cluster has a value of $f_c \simeq 12$ per cent. This result demonstrates that a converged estimate of the star fraction is obtained already at modest resolution with our feedback scheme. This also extends the earlier results by Springel & Hernquist (2003b) to the scale of clusters. Intriguingly, we note that all the runs at very high resolution (VR) even show a small but systematic decrease of the cold gas fraction.

Including feedback from winds has the twofold effect of suppressing the resolution-dependence of the cumulative efficiency and to make the SFR history almost independent of resolution at $z \lesssim 2-3$ (see the right panel of Fig. 3). The enhanced star formation activity at high-redshift of the high resolution runs produces more efficient gas pre-heating, which has the effect of inhibiting star formation at later times. This presumably explains that the star formation rate of the VR run at $z \lesssim 2$ is even below those of the lower-resolution runs. Assuming that the smallest resolved halos where cooling can take place contain ~ 100 DM particles, we find their escape velocity to be of order 100 km s^{-1} for the low-resolution (LR) runs, and a factor of about three smaller for the VR runs of Set #1. Therefore, the wind velocity is always larger than the escape velocity of the smallest halos which are first resolved at high redshift, thereby implying that our feedback scheme is efficient in preventing star formation already in the first generation of resolved galaxies.

An alternative explanation for the decrease of the cold frac-

tion in the VR runs could be that the suppression of star formation in the highest resolution run is related to some numerical effect. For instance, one may argue that an improved resolution provides a more accurate description of the gas behaviour at cooling interface. Indeed, a coarse description of this interface is expected to cause spurious gas cooling (Pearce et al. 1999), a feature that should however be weak in the entropy conserving formulation of SPH (Springel & Hernquist 2002) implemented in our code. However, if this was really the case, one would expect the same effect to appear also in runs without galactic winds (NW runs). But the left panel of Fig. 3 clearly demonstrates that this is not the case. Hence, the stable behaviour of star formation with increasing resolution is more likely related to the inhibiting effect of more efficient high- z feedback onto later generations of galaxies.

The number of identified galaxies within each cluster increases with better resolution and with the cluster mass, as expected. As shown in the right panel of Figure 2, the number of identified *bona-fide* galaxies grows by more than one order of magnitude when passing from the LR to the VR runs. In line with the behaviour of the stellar fraction, the number of galaxies for the CL4 cluster increases by a factor of about three when the wind feedback is switched off, almost independent of the resolution. We defer a detailed analysis of the stellar mass function of the identified galaxies and of the diffuse stellar component as a function of resolution to forthcoming work (Murante et al., in preparation).

In Figure 4, we summarize the results on the star fraction by plotting it as a function of the cluster virial mass, for the reference runs of both Set #1 (filled circles) and of all the 20 clusters of Set #2 (squares). Both simulation sets confirm a trend of decreasing star fraction as a function of the cluster mass. However, clusters belonging to Set #2 show a stellar fraction which is systematically higher than that of Set #1, the difference being larger than any pos-

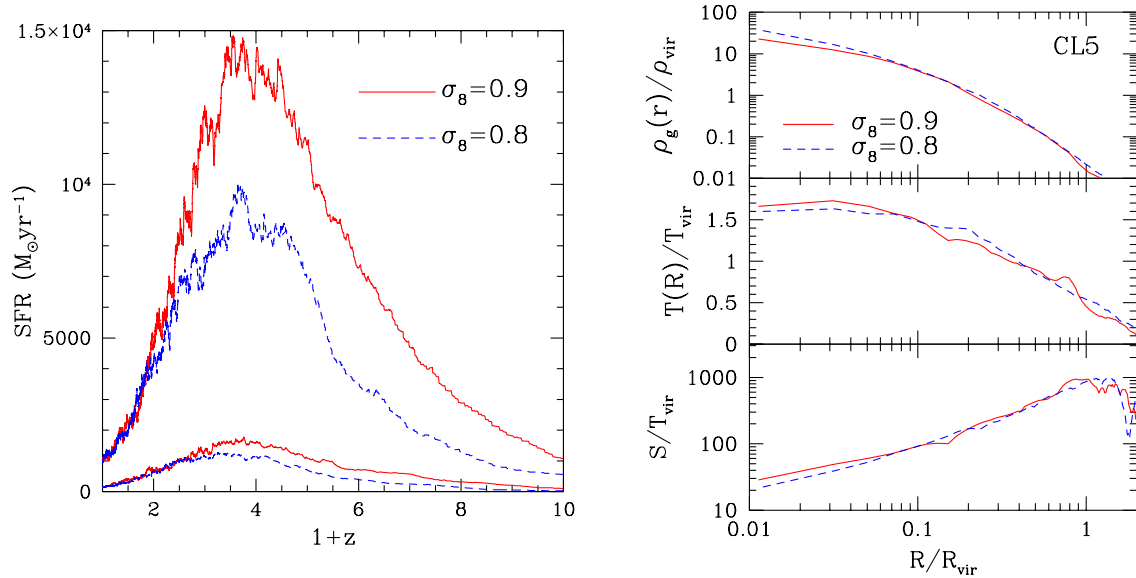


Figure 5. The effect of changing the power spectrum normalization σ_8 . Left panel: the effect on the star-formation history for the CL5 and CL6 clusters (upper and lower pairs of curves), both simulated with the strong-wind (SW) feedback; solid and dashed curves refer to $\sigma_8 = 0.9$ and $\sigma_8 = 0.8$, respectively. Right panel: the effect on gas-related profiles for the CL5 cluster.

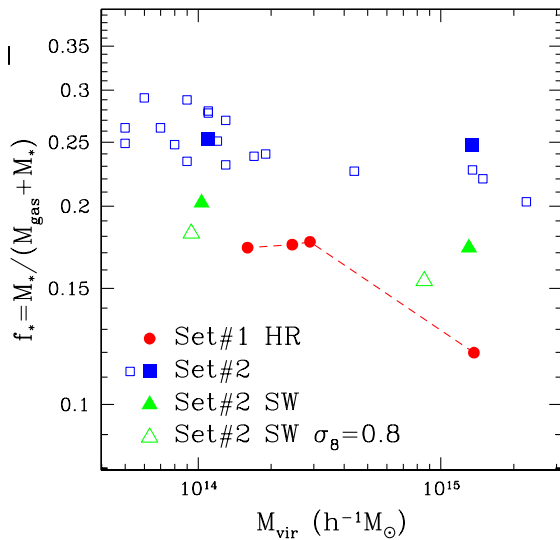


Figure 4. The stellar fraction, f_* , as a function of the cluster virial mass, for the different simulation sets. Filled circles connected by a dashed line are for the high-resolution version of the clusters of Set #1. Squares are for all the clusters of Set #2, with the two filled squares showing the results for simulations CL5 and CL6. Filled triangles are for CL5 and CL6, but using the same velocity of galactic winds, $v_w \simeq 480 \text{ km s}^{-1}$ as for Set #1. The open triangles are the same simulations as the filled triangles, but using the power spectrum normalization of Set #1, $\sigma_8 = 0.8$. Therefore, filled circles and open triangles come from different sets of initial conditions, which however have been evolved using an identical simulation set-up.

sible object-to-object intrinsic scatter induced by the varying dynamical histories of different clusters. However, we recall that the two sets of cluster simulations differ in the strength of the adopted feedback and in the normalization of the power spectrum.

To investigate the effect of the different feedback, we have run additional simulations of CL5 and CL6 of Set #2 by increasing the wind speed to the same value as used for Set #1 (SW runs). The results for the stellar fraction are shown with filled triangles in Fig. 4. Although increasing the feedback efficiency produces a significant suppression of f_* , the effect is still not large enough to fully account for the difference between the two simulation sets, thus suggesting that the residual difference is due to the different σ_8 values.

We have explicitly verified this by repeating the CL5-SW and CL6-SW runs by also decreasing σ_8 to 0.8. The comparison of the resulting star formation histories is shown in the left panel of Figure 5. Reducing σ_8 results in a significant change in the timing of structure formation and, correspondingly, to a delay in the high-redshift star formation, with a suppression of its peak at $z \sim 3$. The resulting stellar fraction further decreases from $f_* = 17.5$ per cent to 15.6 per cent for CL5, and from $f_* = 20.3$ per cent to 18.1 per cent for CL6. As shown in Fig. 4, the reduction of f_* connected to the power spectrum amplitude finally brings the values of the cooled fraction for the simulated clusters of Set #1 and Set #2 into good agreement.

The decreasing trend of the star fraction with cluster mass, shown in Fig. 4, is in qualitative agreement with observational results (Lin et al. 2003; Rines et al. 2004, cf. also Balogh et al. 2001). Lin et al. (2003) used K-band data from the 2MASS survey to trace the stellar population in clusters, and ROSAT-PSPC data to measure the corresponding gas mass. They found $f_* \simeq 10$ per cent for clusters with mass of about $10^{15} h^{-1}M_{\odot}$, increasing to $\simeq 15$ per cent for clusters with $10^{14} h^{-1}M_{\odot}$. These values are not far from those obtained from our runs with stronger feedback and $\sigma_8 = 0.8$. Also, it is worth pointing out that the observational census of the cluster stellar population by Lin et al. (2003) does not include diffuse stars, whose contribution may not be negligible both for real (e.g., Arnaboldi 2004, for a review) and simulated (Murante et al. 2004; Willman et al. 2004; Sommer-Larsen et al.

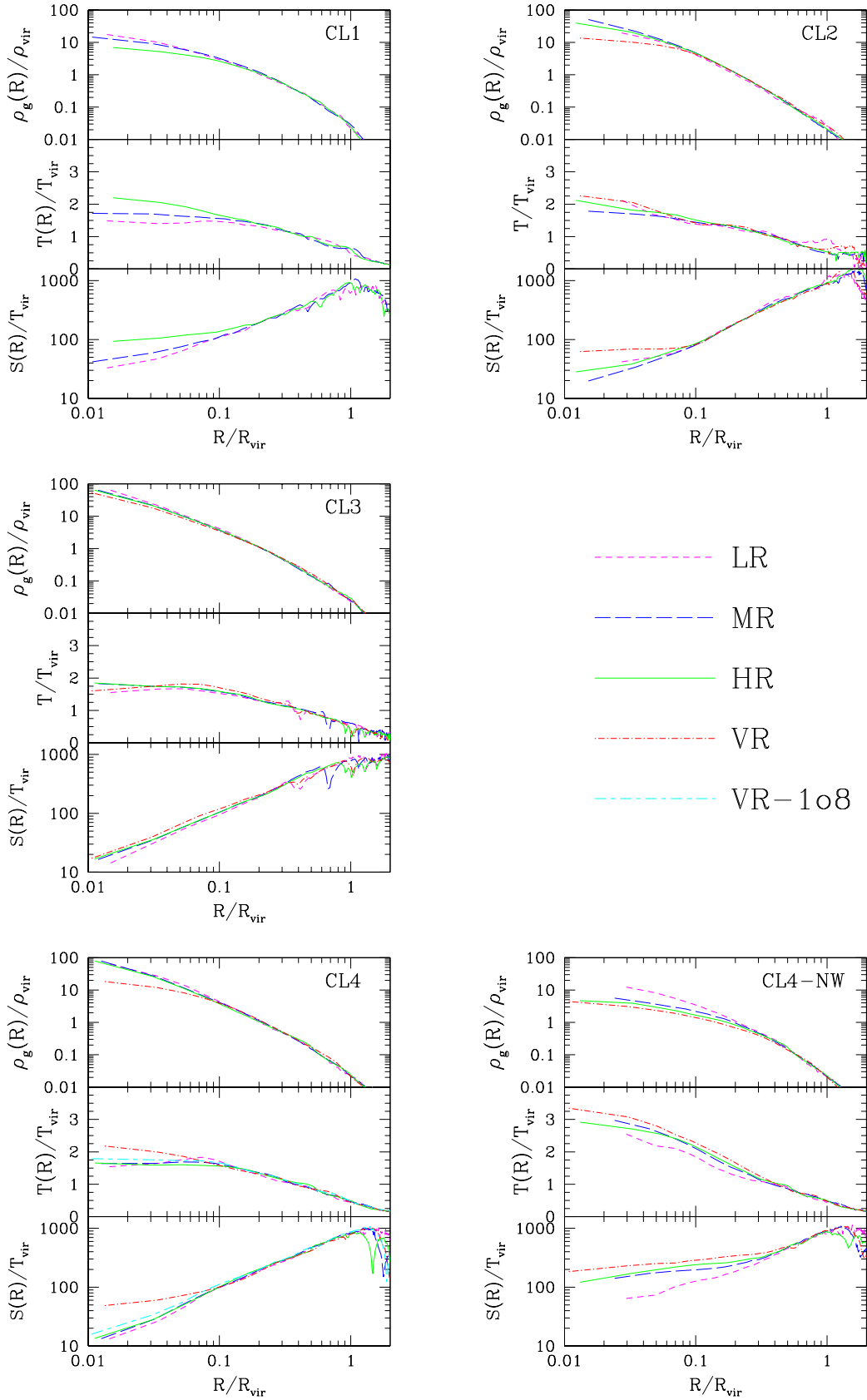


Figure 6. The effect of resolution on the profiles of gas density, temperature and entropy (from top to bottom in each panel). Each panel shows the profiles for the different resolutions at which each cluster of Set #1 has been simulated. For the CL4 cluster, we also show the results for the series of runs where the effect of winds has been excluded (NW).

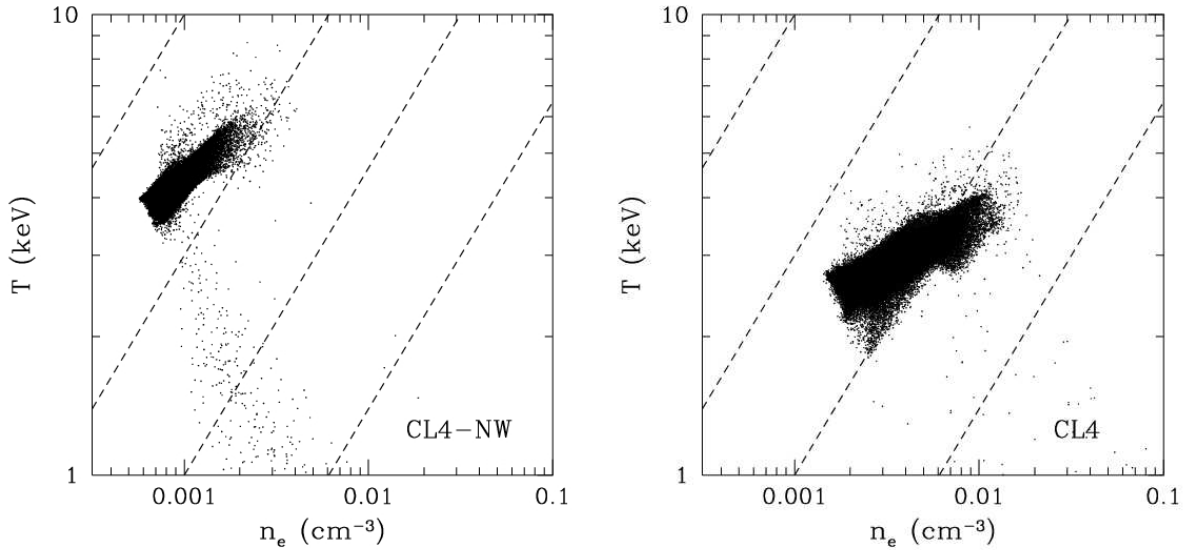


Figure 7. The distribution of gas particles for the very high-resolution (VR) version of the CL4 cluster, lying within $0.1R_{\text{vir}}$ around the centre, in the n_e - T plane (n_e and T : electron number density and temperature of each gas particle, in units of cm^{-3} and keV, respectively). Left and right panels are for the run without and with the effect of galactic winds, respectively. In each panel, the dashed curves indicate levels of constant entropy ($S = 1000, 300, 100$, and 30 keV cm^2 , from upper to lower curves).

2005) clusters. Note that our estimates of f_* include all stars found inside the simulated clusters.

How do our results compare with previous simulations? An overproduction of stars in simulations including radiative physics has been a well established result for several years (e.g., Katz & White 1993; Sugihara & Ostriker 1998; Lewis et al. 2000; Davé et al. 2002). This problem is generally thought to be solved by a physical feedback process, which prevents excessive gas cooling with a continuous energy supply. However, realistically modelling such a heating process is a difficult problem. For instance, Tornatore et al. (2003) verified that using thermal feedback instead of the kinetic one applied here, the fraction of cooled baryons is of order 30 per cent, with no evidence for convergence with better numerical resolution. Muanwong et al. (2002) claimed that overcooling within clusters can be eventually avoided by suitably pre-heating gas at high redshift. Kay et al. (2004) implemented a scheme of thermal feedback which increases the entropy of gas particles which are just undergoing cooling. Although this feedback is tuned to reproduce several X-ray observational properties of clusters, it still provides a too large star fraction, of about $\simeq 25$ per cent. While all these results are based on SPH codes, Kravtsov et al. (2005) used an adaptive Eulerian code, which also includes cooling, star formation and thermal feedback. They find rather large stellar fractions as well, with values of about 30–40 per cent within the cluster virial radius, which is consistent with the SPH simulations.

3.2 Thermodynamics of the hot gas

In Figure 6, we show the radial profiles of gas density, temperature, and entropy, for the the four clusters the Set #1, at different resolutions. We find that the profiles are rather stable against resolution on scales $R \gtrsim 0.1R_{\text{vir}}$. On smaller scales, where the complex physics of cooling, star formation and winds’ feedback plays a significant role, we detect significant systematic changes of the profiles with

increasing resolution. In general, the gas density and entropy profiles become slightly shallower, and the temperature profiles somewhat steeper, as the resolution is increased. The size of this effect changes from object to object, depending on the different dynamical histories, being more apparent for the CL1 cluster and rather small for the CL3 cluster.

Shallower gas-density and entropy profiles can be due either to more efficient non-gravitational heating from energy feedback or to more efficient radiative cooling. In the first case, the stronger heating places gas on a higher adiabat, thereby preventing it from reaching high density in the central halo region (e.g. Tozzi & Norman 2001, and references therein). In the second case, a more efficient cooling turns into a more efficient selective removal of low entropy gas from the hot phase (e.g., Voit & Bryan 2001). As a result, the gas density decreases, while leaving behind the hot phase at its relatively higher entropy. If cooling is the process that governs the resolution-dependence of the profiles, we would expect a more efficient star formation and a larger fraction of cooled gas at increasing resolution. However, this is not found for the runs including galactic winds (see Figs. 2 and 3). On the other hand, increasing the resolution has the effect of increasing star formation efficiency and, therefore, the amount of feedback energy released to the gas at high redshift. Indeed, galactic winds are expected to be more efficient at high redshift, when they can more easily escape from shallower potential wells. Better resolution hence increases the gas heating associated with high-redshift star formation.

The inner slope of the temperature profiles obtained in radiative simulations is known to be significantly steeper than observed for real clusters (e.g., Borgani et al. 2004, cf. also Kay et al. 2004). This effect has been interpreted as being due to the adiabatic compression of gas which falls in from outer cluster regions, as a consequence of the reduced pressure support after removal of cooled gas. Our results show that improving resolution does not help to reconcile simulated and observed temperature profiles. In fact, this

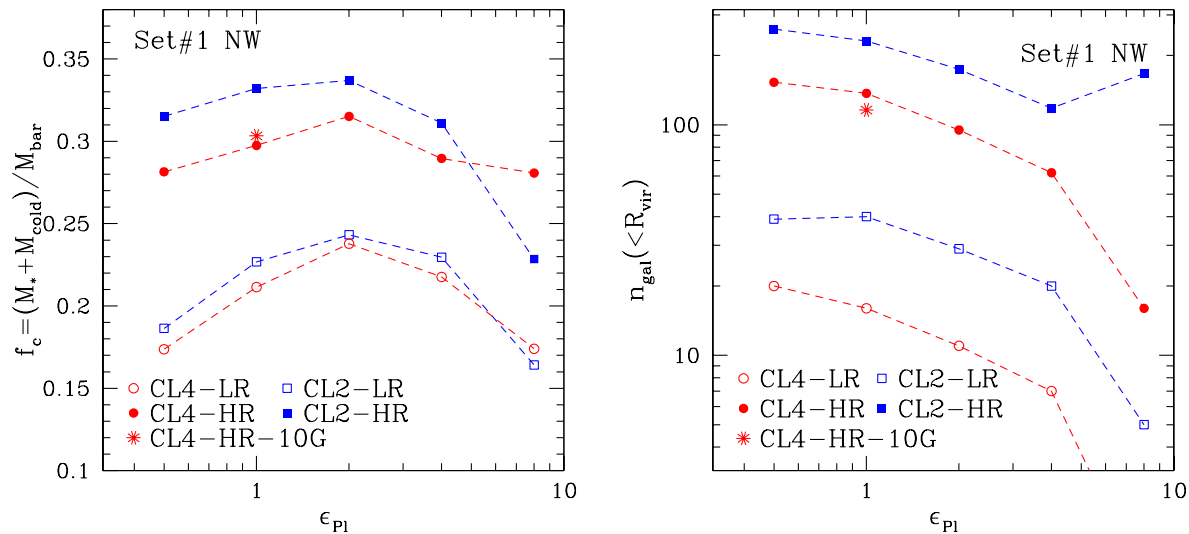


Figure 8. The fraction of cooled baryons (left panel) and the number of galaxies (right panel) within the virial radius, as a function of the gravitational softening, for the CL2 and CL4 clusters (both in the LR and HR version). The softening is given in units of the value assumed for the reference runs (see Table 2). These simulations did not include galactic winds (NW runs).

discrepancy can become even worse with better numerical resolution.

In Fig. 6, we show profiles of the gas properties for the CL4 runs with no winds (NW). Also for these runs, we note similar trends with resolution as for the runs including feedback by winds. However, in this case the increase of the central entropy level, and the corresponding decrease of the gas density, are explained by the higher efficiency of cooling with better resolution. Therefore, although the runs with and without feedback by winds show similar trends with resolution, the interpretation of these effects is completely different in the two cases.

Furthermore, a comparison of the CL4 runs with and without winds shows that, at fixed resolution, the former have higher central density, shallower temperature profiles and lower entropy levels. In order to explicitly demonstrate the effect of feedback on the gas thermodynamics in the central cluster regions, we show in Figure 7 a phase diagram of the gas particles lying within the central $0.1R_{\text{vir}}$ for the CL4 cluster, with and without feedback by galactic winds. Perhaps somewhat counterintuitively, the effect of feedback is that of lowering the typical temperature of the gas in the central cluster regions, and shifting it to a lower adiabat. This result emphasizes the role of feedback in the central cluster regions: a continuous supply of energy by feedback has the effect of keeping a population of relatively low-entropy gas particles in the hot phase, which have a short enough cooling time that they would otherwise have dropped out of the hot phase and cooled onto the centre. The presence of such gas particles explains the higher gas density and the lower entropy level. Furthermore, the higher pressure support associated with the feedback energy reduces the compressional heating of in-falling gas and, as a consequence, the ICM temperature in the central cluster regions.

Observational data on the temperature structure in cool-core clusters indicate that the ICM reaches there a lower limiting temperature which is about 1/2–1/4 of the overall cluster virial temperature (e.g., Peterson et al. 2001; Molendi & Pizzolato 2001; Böhringer et al. 2002). The generally accepted interpretation is that

some sort of feedback prevents gas from reaching lower temperature by compensating its radiative losses, thus suppressing also the cooling rate. Our results on the effect of feedback in simulations clearly corroborates this picture. However, our implemented feedback is still not efficient enough to suppress the cooling rate and, correspondingly, the compressional heating to the observed level. As a consequence, the temperature profiles in the central regions are still steeper than observed, and no cool cores are created.

Finally, we consider the effect of changing σ_8 on the profiles of gas-related quantities (right panel of Fig. 5). We find that the gas properties are left almost unchanged, once they are rescaled to compensate for the difference in virial temperature. However, slightly shallower density and entropy profiles, and a slightly steeper temperature profile characterize the runs with $\sigma_8 = 0.9$. This can be understood as a consequence of the enhanced cooling, which removes a larger fraction of gas from the hot phase in the central cluster regions and, correspondingly, increases the compressional heating of the in-flowing gas.

4 THE EFFECT OF NUMERICAL HEATING

4.1 Changing the gravitational softening

The choice for the gravitational softening is a compromise between the goal of resolving the smallest scales possible and the need to ensure that the relaxation time by two-body interactions is much larger than the typical age of the simulated structure (e.g. Thomas & Couchman 1992). Using a very small softening may allow one to resolve a larger number of small halos, but this comes at the price of introducing spurious numerical heating of the gas, which could artificially suppress cooling. Therefore, by increasing the softening we expect to first see a more efficient cooling, until a point is reached when only large halos, with their comparatively long cooling times, are resolved and the cooling efficiency declines again. This implies that a softening value should exist which max-

imizes the amount of cooled gas, while smaller and larger values lead to less cold gas as a result of spurious gas heating or lack of resolution, respectively.

To check for this effect, we show in Figure 8 the dependence of the fraction of cooled baryons, f_c , and of the number of identified galaxies n_{gal} within the virial radius on the adopted gravitational softening length. We show results both for the low-resolution (LR) and the high-resolution (HR) versions of the CL2 and CL4 clusters. In order to avoid mixing the effects of numerical heating with that of efficient feedback, we have performed these simulations by switching off feedback by galactic winds (NW). In the plot of Figure 8, the softening is given in units of that adopted for our reference simulations, as reported in Table 2. The results clearly confirm our expectation: both a too large and a too small softening lead to a decrease of the amount of cooled gas. Quite interestingly, the softening (in units of the reference value) at which the cooled baryon fraction is maximised is the same at low and high resolution. This demonstrates that the adopted scaling of the softening length with mass resolution, $\epsilon_{\text{P1}} \propto m_{\text{gas}}^{1/3}$ is in fact a reasonable choice.

In general, we find that the maximum value of f_c is attained for a softening value about twice as large as our reference value. This implies that a two times larger softening should then be preferred, although the difference in f_c when using $\epsilon_{\text{P1}} = 1$ instead of 2 is always rather small, especially at high mass resolution.

As for the number of identified galaxies, it monotonically decreases with increasing softening (right panel of Fig. 8). Using $\epsilon_{\text{P1}} = 2$ provides a ~ 30 per cent smaller number of galaxies than for $\epsilon_{\text{P1}} = 1$. However, this argument does not necessarily represent a valid support for the choice of a smaller softening. Indeed, a spurious energy transfer from DM to gas may lead to a tightening of the DM halos, thereby producing a larger number of small halos. Clearly, a close investigation of the optimal strategy to minimize the effect of numerical heating would require a more detailed analysis than that presented here, including a close investigation of the mass function of the resolved galaxies. We plan to present this analysis in a forthcoming paper.

We finally note that the anomalous number of galaxies for the HR version of the CL2 cluster is apparently a result of a misclassification by SKID, as we checked by visual inspection. Here, the distribution of star particles shows that they are arranged in a few over-merged galaxies, most of which have pretty large tidal tails. The SKID algorithm sometimes splits these tails into separate gravitationally bound structures, which are then misclassified as galaxies.

As a further test, we have compared the results of the CL6 run with strong winds, assuming $z = 2$ and $z = 5$ for the redshift of transition from comoving to physical softening. As shown in Figure 9 the smaller high- z softening provides an enhanced efficiency of star formation. In this case, the cooling efficiency within small resolved halos dominates over the effect of numerical heating in defining the pattern of star formation.

4.2 Gas-DM particle splitting

As we have already discussed, heating of gas particles from two-body encounters may spuriously alter the thermodynamic properties of the gas. Based on an estimate of the heating time from two-body encounters in the impulse approximation (Binney & Tremaine 1987), Steinmetz & White (1997) analytically derived the heating time associated with such encounters. Un-

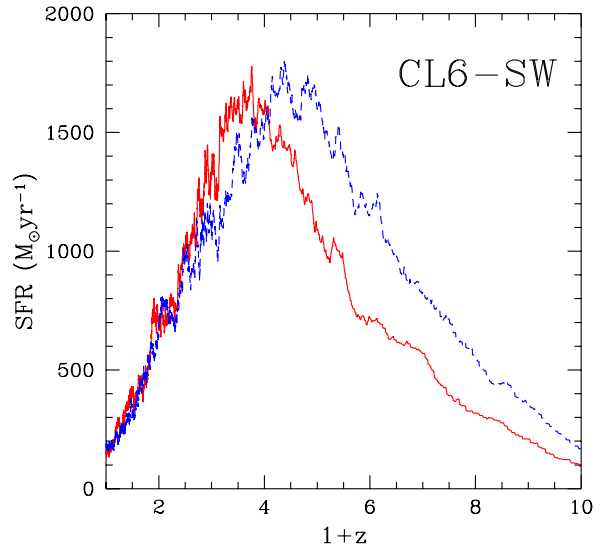


Figure 9. Comparison of the results for the CL6 cluster using both $z = 5$ (solid line) and $z = 2$ (dashed line) for the transition redshift from physical to comoving softening. Strong winds (SW) have been included in these simulations.

der the assumption of hydrostatic equilibrium, this heating time is inversely proportional to the mass of the DM particle, while being independent of the gas particle mass. As a consequence, a limiting mass of DM particles can be derived for two-body heating rate to dominate over the cooling rate within a given halo, as a function of the virial temperature of the halo itself. According to their results, the mass resolution achieved in our runs, with the possible exception of the low-resolution (LR) series for clusters of Set #1, should be adequate to prevent spurious heating within halos having temperature of at least few keV. While this holds for already formed halos at low redshift, the situation may be different at high redshift, when gas cooling takes place within small, just resolved galaxy-sized halos. Also, in the first generation of halos, substantial residual gas motions exist which could give rise to an additional artificial energy transfer in two-body encounters from the heavier DM particles to the lighter gas particles.

In order to reduce the amount of numerical heating from such energy equipartition effects one may try to increase the number of DM particles, thereby decreasing their mass, while keeping the mass resolution of the gas fixed. In order to check for this effect, we resimulated the CL4 halo assuming very high resolution (VR) for the DM particles. However, in this case we generated initial displacements for an eight times smaller number of gas particles (108 runs in Table 3). In this way, gas and DM particles have a comparable mass: $m_{\text{gas}}/m_{\text{DM}} \simeq 1.06$ instead of $\simeq 0.15$. In terms of gas-mass resolution, this simulation is intermediate between the MR and HR runs, but with a more accurate treatment of gravity, thanks to the larger number of DM particles, which should suppress numerical heating.

In Fig. 2, we show the effect on the cooled gas fraction and on the number of formed galaxies with the asterisks. Quite interestingly, the resulting cooled fraction is very similar to that obtained for the MR and HR runs of the same cluster. As for the number of resolved galaxies, it is close to that obtained for the corresponding HR run, which has anyway a better gas-mass resolution. This increase in the number of identified galaxies inside the cluster can have two possible explanations. It is either due to an intrinsic in-

crease of the number of resolved halos where gas cooling takes place, or to an improved capability of small halos to survive disruption in the cluster tidal field. To check this, we compare the values of $n_{\text{gal}}(< R_{\text{vir}})$ inside the cluster with the corresponding number of galaxies in the region $R_{\text{vir}} < R < 4R_{\text{vir}}$ around the cluster. Within R_{vir} , we identify 56 galaxies for the HR run and 53 galaxies for the 1o8 run. However, the difference between the two runs increases significantly in the outer cluster regions, with 123 galaxies found for the HR run and 75 for the 1o8 run. This shows that the better gas–mass resolution of the HR run in fact produces a larger number of galaxies in the field, while the improved accuracy in the gravitational force computation for the 1o8 run compensates for this effect within clusters, where it plays a significant role in preventing tidal disruption of small galaxies.

With respect to the cosmic star–formation history, the 1o8 run (heavy solid curve in Fig. 3) shows a behaviour which is not strictly intermediate between MR and HR runs. The onset of star formation takes place at a higher redshift than in the HR runs, and then proceeds in a more efficient way. Quite remarkably, the peak of star formation is even higher than for the highest resolution (VR) run. Finally, results of the 1o8 run for the gas profiles are shown with the long–short–dashed curve in the bottom left panel of Fig. 6. Much like for the results on the cooled gas fraction, the resulting profiles are very similar to those of the MR and HR runs.

Overall, the test on the degree of spurious gas heating from two–body relaxation confirms that a DM particle mass of at most $\simeq 10^9 h^{-1} M_{\odot}$ is sufficient to provide a reliable description of gas cooling within an already formed cluster of galaxies at low redshift. However, increasing the DM mass–resolution in order to reduce numerical heating of the gas from two–body encounters has a non–negligible effect on the number of resolved galaxies and on the star formation history, as a result of the better resolution of early structure formation. The comparatively low computational cost of the gravity part in a hydrodynamical simulation with radiative cooling, and the availability of large amounts of memory in modern supercomputers, may make it attractive to adopt a larger number of DM particles than gas particles in future simulation work.

4.3 Grid vs. glass initial conditions

As we discussed in Section 2, the initial Lagrangian particle distributions of the simulations of Set #1 have been realized as a grid, while those of Set #2 have been a glass. The glass–based technique to generate initial conditions (ICs; White 1996) aims at suppressing effects due to the regularity of the initial grid, which amplifies structure at the scale of the mean–interparticle separation. In the glass scheme, particle positions are initially generated randomly in the simulation box, but are then evolved backwards in time until they reach an amorphous, minimum energy configuration where each particle experiences only vanishingly small forces. The resulting irregular particle distribution lacks preferred directions and should be less affected by the symmetries that occur in the grid method.

In order to check the effect of using either one of the two techniques to generate ICs, we have rerun the CL5 cluster with strong winds (SW), but this time starting from grid displacements. The results of this test are shown in Figure 10, where we plot the corresponding star–formation histories (left panel) and the radial profiles of gas properties (right panels). This comparison demonstrates that, at least at the resolution relevant for our simulations, the difference between using grid or glass ICs is very small. Looking at the details of the comparison, it turns out that the grid–based run has a

slightly higher star–formation at $z \gtrsim 6$. This may be due to a contribution of the small–scale fluctuation modes around the Nyquist frequency, which should collapse more efficiently in the grid case (and part of this may be artificial), favoring somewhat earlier cooling at high– z . However, the star fractions within the cluster virial radius at $z = 0$ are $f_* = 0.17$ for both runs. The number of identified galaxies within the same region is 412 and 380 for the grid and glass runs, respectively. This appears to confirm that grid–based ICs show slightly higher power on small scales, which, in turn, generates a slightly larger number of galaxies. As for the profiles of gas related quantities, we note that they also overlap quite closely. The only noteworthy difference is that the positions of merging substructures vary. However, such differences in orbital timing are expected and common when different methods for the generation of ICs are used.

The general result of this comparison is that, at least at the resolution relevant for our cluster simulations, the effect of using either grid or glass ICs is very small, in any case negligible with respect to other numerical effects that we have explored in this paper.

5 CONCLUSIONS

In this paper we have presented results from a large set of hydrodynamical simulations of galaxy clusters, carried out with the Tree+SPH code GADGET-2. Our simulations include radiative cooling, star formation and energy feedback by a phenomenological model for galactic winds. The main target of our analysis has been the study of the stability of simulation results with respect to numerical parameters, such as mass resolution or gravitational softening length. We also considered different sources of numerical heating, and their interplay with the complex physical effects included. As such, our analysis also represents a validation study of our previous results (e.g., Borgani et al. 2004), which were based on a large cosmological box simulated at a relatively low resolution.

Our simulated clusters span more than one order of magnitude in collapsed mass and several decades in mass resolution. At the highest resolution, the mass of the gas particles is $m_{\text{gas}} \simeq 1.5 \times 10^7 h^{-1} M_{\odot}$, which allows us to resolve the virial region of a Virgo–like cluster with more than 2 million gas particles and at least as many dark–matter (DM) particles. Our main results are concerned with the effects of resolution on the properties of the stellar populations and on the intra–cluster medium of the simulated galaxy clusters. They can be summarized as follows.

(a) In the absence of an efficient energy feedback, the fraction of cooled baryons steadily increases with resolution, reaching $\simeq 35$ per cent at the highest achieved resolution (VR runs in Table 2), with no indication for convergence.

(b) Including feedback from galactic winds has the effect of stabilizing the stellar fraction inside clusters. Assuming a high efficiency for the supernova driven winds of order unity, we find that the fraction of cooled baryons converges already at a relatively modest resolution, with an indication to decrease very slightly at the highest resolution. This arises as a consequence of the self–regulation property of star formation and feedback. While improving the resolution increases the star formation efficiency at very high redshift, this at the same time also provides a significant contribution to gas pre–heating which reduces star formation later on. The fraction of cooled baryons within R_{vir} lies in the range 12–18 per cent, with a decreasing trend with cluster mass. These values increase by about 15 per cent when the normalization of the power–spectrum is raised from $\sigma_8 = 0.8$ to 0.9.

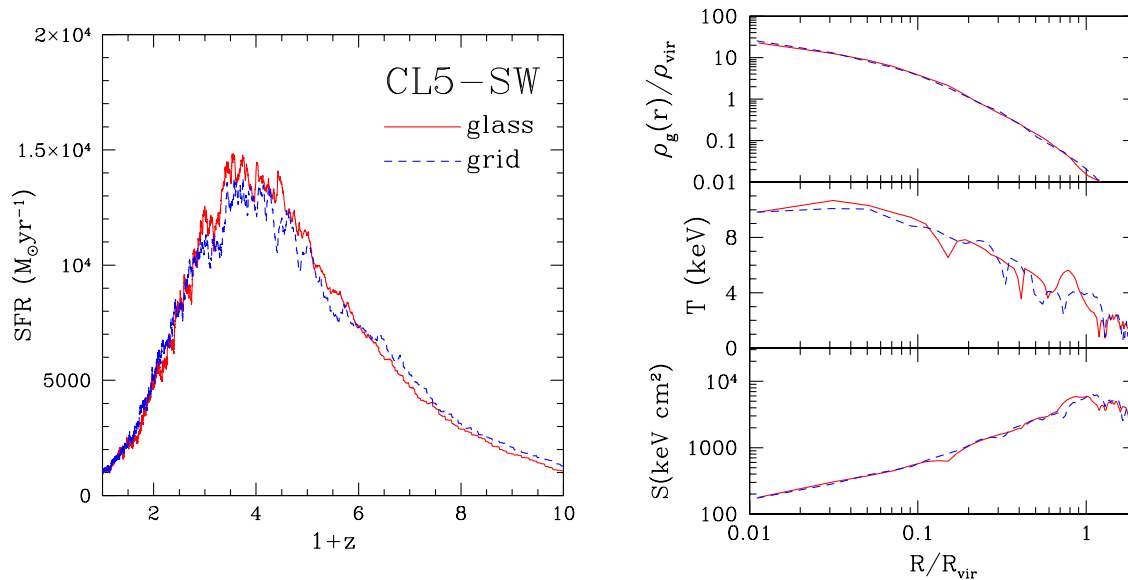


Figure 10. Comparison of the results for the CL5 cluster using both glass (solid lines) and grid (dashed lines) initial conditions. The left panel is for the redshift dependence of the star formation rate, while the right panels show the profiles of gas density, temperature, and entropy. Strong winds (SW) have been included in these simulations.

(c) The feedback provides the necessary continued energy supply to keep gas particles of comparately low entropy and short cooling times in the hot phase of clusters, while without feedback these particles would cool down and drop out of the cluster atmosphere. As a result, the central gas density is higher in runs with feedback than in the runs with no galactic winds. The temperature profiles are shallower in the central cluster regions, while isentropic cores are much less pronounced, thus alleviating the discrepancy with the observed properties of the intra-cluster medium.

A further series of tests presented in this paper concerns the effect of numerical heating. The main results from these tests can be summarized as follows.

(a) Our Plummer-equivalent force softening of $\epsilon_{\text{PI}} \simeq 10 h^{-1} \text{kpc}$ at a mass resolution of $m_{\text{DM}} \simeq 5 \times 10^9 h^{-1} M_{\odot}$, scaled to other particle masses as $\epsilon_{\text{PI}} \propto m_{\text{DM}}^{1/3}$, represents a reasonable compromise between the need of preventing a spurious numerical heating of the gas, and the desire to resolve galaxies in the largest possible number of small DM halos.

(b) Increasing the mass resolution in the DM component while keeping the gas mass resolution fixed, helps to reduce numerical gas heating by two-body encounters (Steinmetz & White 1997). We find that decreasing m_{DM} has a negligible effect on the fraction of cooled gas at $z = 0$ and on the radial profiles of gas properties. However, it has a non-negligible effect on the star formation history, which occurs with enhanced efficiency at $z \gtrsim 3$. This is the result both of a non-negligible numerical heating in small halos when gas and DM particles have rather different masses, and also of a better resolved dark matter content in the first generation of halos.

In sum, our analysis helps to establish and delineate the regime of numerical reliability of the present generation of hydrodynamical SPH simulations of galaxy clusters. Even though quite technical in nature, it is clear that systematic tests like the ones discussed here are required to elucidate the often delicate interplay

between numerical effects and the physical model that is studied. Only when these effects are understood, the predictive power of numerical experiments can be fully exploited. At the same time, this understanding is also required to successfully push to new generations of simulations with yet higher resolution. A reassuring aspect of the results discussed here is that even simulation models with complex and highly non-linear physical models for star formation and feedback can produce surprisingly robust results. This clearly is an encouragement for attempts to improve the fidelity with which the physics is represented in future simulation work.

ACKNOWLEDGEMENTS

The simulations were carried out on the IBM-SP4 machine and on the IBM-Linux cluster at the ‘‘Centro Interuniversitario del Nord-Est per il Calcolo Elettronico’’ (CINECA, Bologna), with CPU time assigned under INAF/CINECA and University-of-Trieste/CINECA grants, on the IBM-SP3 at the Italian Centre of Excellence ‘‘Science and Applications of Advanced Computational Paradigms’’, Padova and on the IBM-SP4 machine at the ‘‘Rechenzentrum der Max-Planck-Gesellschaft’’, Garching. This work has been partially supported by the PD-51 INFN grant. We wish to thank an anonymous referee for his/her comments which helped improving the presentation of the results.

REFERENCES

- Arnaboldi M., 2004, in IAU Symposium Intracluster Stellar Population, pp 54–+
- Arnaud M., Evrard A. E., 1999, MNRAS, 305, 631
- Böhringer H., Matsushita K., Churazov E., Ikebe Y., Chen Y., 2002, A&A, 382, 804
- Babul A., Balogh M. L., Lewis G. F., Poole G. B., 2002, MNRAS, 330, 329

- Balogh M. L., Pearce F. R., Bower R. G., Kay S. T., 2001, *MNRAS*, 326, 1228
- Binney J., Tremaine S., 1987, *Galactic dynamics*. Princeton, NJ, Princeton University Press, 1987, 747 p.
- Borgani S., Governato F., Wadsley J., Menci N., Tozzi P., Quinn T., Stadel J., Lake G., 2002, *MNRAS*, 336, 409
- Borgani S., Murante G., Springel V., Diaferio A., Dolag K., Moscardini L., Tormen G., Tornatore L., Tozzi P., 2004, *MNRAS*, 348, 1078
- Bower R. G., Benson A. J., Lacey C. G., Baugh C. M., Cole S., Frenk C. S., 2001, *MNRAS*, 325, 497
- Cheng L.-M., Borgani S., Tozzi P., Tornatore L., Diaferio A., Dolag K., He X.-T., Moscardini L., Murante G., Tormen G., 2005, *A&A*, 431, 405
- Davé R., Katz N., Weinberg D. H., 2002, *ApJ*, 579, 23
- Diaferio A., Borgani S., Moscardini L., Murante G., Dolag K., Springel V., Tormen G., Tornatore L., Tozzi P., 2005, *MNRAS*, 356, 1477
- Dolag K., Jubelgas M., Springel V., Borgani S., Rasia E., 2004, *ApJ*, 606, L97
- Eke V. R., Cole S., Frenk C. S., 1996, *MNRAS*, 282, 263
- Ettori S., Borgani S., Moscardini L., Murante G., Tozzi P., Diaferio A., Dolag K., Springel V., Tormen G., Tornatore L., 2004, *MNRAS*, 354, 111
- Ettori S., De Grandi S., Molendi S., 2002, *A&A*, 391, 841
- Ettori S., Dolag K., Borgani S., Murante G., 2005, *ArXiv Astrophysics e-prints*
- Frenk C. S., White S. D. M., Bode P., et al. 1999, *ApJ*, 525, 554
- Haardt F., Madau P., 1996, *ApJ*, 461, 20
- Kaiser N., 1986, *MNRAS*, 222, 323
- Kang H., Ostriker J. P., Cen R., Ryu D., Hernquist L., Evrard A. E., Bryan G. L., Norman M. L., 1994, *ApJ*, 430, 83
- Katz N., White S. D. M., 1993, *ApJ*, 412, 455
- Kay S. T., Pearce F. R., Frenk C. S., Jenkins A., 2002, *MNRAS*, 330, 113
- Kay S. T., Thomas P. A., Jenkins A., Pearce F. R., 2004, *MNRAS*, 355, 1091
- Kravtsov A. V., Nagai D., Vikhlinin A. A., 2005, *ApJ*, 625, 588
- Lapi A., Cavaliere A., Menci N., 2005, *ApJ*, 619, 60
- Lewis G. F., Babul A., Katz N., Quinn T., Hernquist L., Weinberg D. H., 2000, *ApJ*, 536, 623
- Lin Y.-T., Mohr J. J., Stanford S. A., 2003, *ApJ*, 591, 749
- Markevitch M., 1998, *ApJ*, 504, 27
- Molendi S., Pizzolato F., 2001, *ApJ*, 560, 194
- Muanwong O., Thomas P. A., Kay S. T., Pearce F. R., 2002, *MNRAS*, 336, 527
- Murante G., Arnaboldi M., Gerhard O., Borgani S., Cheng L. M., Diaferio A., Dolag K., Moscardini L., Tormen G., Tornatore L., Tozzi P., 2004, *ApJ*, 607, L83
- Navarro J. F., Frenk C. S., White S. D. M., 1995, *MNRAS*, 275, 720
- O'Shea B. W., Nagamine K., Springel V., Hernquist L., Norman M. L., 2005, *ApJS*, 160, 1
- Osmond J. P. F., Ponman T. J., 2004, *MNRAS*, 350, 1511
- Pearce F. R., Jenkins A., Frenk C. S., Colberg J. M., White S. D. M., Thomas P. A., Couchman H. M. P., Peacock J. A., Efstathiou G., The Virgo Consortium 1999, *ApJ*, 521, L99
- Pearce F. R., Thomas P. A., Couchman H. M. P., Edge A. C., 2000, *MNRAS*, 317, 1029
- Peterson J. R., Paerels F. B. S., Kaastra J. S., Arnaud M., Reiprich T. H., Fabian A. C., Mushotzky R. F., Jernigan J. G., Sakelliou I., 2001, *A&A*, 365, L104
- Ponman T. J., Sanderson A. J. R., Finoguenov A., 2003, *MNRAS*, 343, 331
- Power C., Navarro J. F., Jenkins A., Frenk C. S., White S. D. M., Springel V., Stadel J., Quinn T., 2003, *MNRAS*, 338, 14
- Rines K., Geller M. J., Diaferio A., Kurtz M. J., Jarrett T. H., 2004, *AJ*, 128, 1078
- Rosati P., Borgani S., Norman C., 2002, *ARAA*, 40, 539
- Salpeter E. E., 1955, *ApJ*, 121, 161
- Shandarin S. F., Zeldovich Y. B., 1989, *Reviews of Modern Physics*, 61, 185
- Sommer-Larsen J., Romeo A. D., Portinari L., 2005, *MNRAS*, 357, 478
- Springel V., 2005, *ArXiv Astrophysics e-prints*
- Springel V., Hernquist L., 2002, *MNRAS*, 333, 649
- Springel V., Hernquist L., 2003a, *MNRAS*, 339, 289
- Springel V., Hernquist L., 2003b, *MNRAS*, 339, 312
- Springel V., Yoshida N., White S., 2001, *New Astronomy*, 6, 79
- Stadel J. G., 2001, *Ph.D. Thesis*
- Steinmetz M., White S. D. M., 1997, *MNRAS*, 288, 545
- Suginohara T., Ostriker J. P., 1998, *ApJ*, 507, 16
- Thomas P. A., Couchman H. M. P., 1992, *MNRAS*, 257, 11
- Tormen G., Bouchet F. R., White S. D. M., 1997, *MNRAS*, 286, 865
- Tornatore L., Borgani S., Springel V., Matteucci F., Menci N., Murante G., 2003, *MNRAS*, 342, 1025
- Tozzi P., Norman C., 2001, *ApJ*, 546, 63
- Voit G. M., 2005, *Reviews of Modern Physics*, 77, 207
- Voit G. M., Balogh M. L., Bower R. G., Lacey C. G., Bryan G. L., 2003, *ApJ*, 593, 272
- Voit G. M., Bryan G. L., 2001, *Nature*, 414, 425
- White S., 1996, in Schaeffer R., Silk J., Spiro M., Zinn-Justin J., eds, *Cosmology and Large-Scale Structure The formation and evolution of galaxies*. Elsevier, Dordrecht, p. 395
- Willman B., Governato F., Wadsley J., Quinn T., 2004, *MNRAS*, 355, 159
- Yoshida N., Sheth R. K., Diaferio A., 2001, *MNRAS*, 328, 669
- Yoshida N., Stoehr F., Springel V., White S. D. M., 2002, *MNRAS*, 335, 762
- Zhan H., 2005, *ArXiv Astrophysics e-prints*